AGU PUBLICATIONS

Geophysical Research Letters

RESEARCH LETTER
10.1002/2015GL064236

Key Points:
- Greenland glaciers are undercut by the ocean
- Echo sounding observations challenge current knowledge
- Undercutting must play a major role in the glacier evolution

Supporting Information:
- Readme
- Figure S1
- Figure S2
- Figure S3
- Figure S4
- Figure S5

Correspondence to:
E. Rignot,
erignot@uci.edu

Citation:
Rignot, E., I. Fenty, Y. Xu, C. Cai, and C. Kemp (2015), Undercutting of marine-terminating glaciers in West Greenland, *Geophys. Res. Lett.*, *42*, 5909–5917, doi:10.1002/2015GL064236.

Received 8 MAY 2015
Accepted 25 JUN 2015
Accepted article online 30 2015
Published online 27 JUL 2015

Undercutting of marine-terminating glaciers in West Greenland

Eric Rignot[1,2], Ian Fenty[2], Yun Xu[1], Cilan Cai[1], and Chris Kemp[3]

[1]Department of Earth System Science, University of California, Irvine, California, USA, [2]Jet Propulsion Laboratory, Pasadena, California, USA, [3]Terrasond Ltd., Seattle, Washington, USA

Abstract Marine-terminating glaciers control most of Greenland's ice discharge into the ocean, but little is known about the geometry of their frontal regions. Here we use side-looking, multibeam echo sounding observations to reveal that their frontal ice cliffs are grounded deeper below sea level than previously measured and their ice faces are neither vertical nor smooth but often undercut by the ocean and rough. Deep glacier grounding enables contact with subsurface, warm, salty Atlantic waters (AW) which melts ice at rates of meters per day. We detect cavities undercutting the base of the calving faces at the sites of subglacial water (SGW) discharge predicted by a hydrological model. The observed pattern of undercutting is consistent with numerical simulations of ice melt in which buoyant plumes of SGW transport warm AW to the ice faces. Glacier undercutting likely enhances iceberg calving, impacting ice front stability and, in turn, the glacier mass balance.

1. Introduction

Increased surface melting of the Greenland Ice Sheet and enhanced flow of its marine-terminating glaciers have significantly contributed to sea level rise in the past two decades [e.g., *Ettema et al.*, 2009; *Rignot et al.*, 2011]. At the ice-ocean interface, marine-terminating glaciers interact with a shallow layer of fresh Polar Water (PW) in the upper 150–200 m and, if sufficiently deep, a denser layer of relatively warm and salty Atlantic Water (AW) below 200 m [*Straneo et al.*, 2013]. The transport of AW to the glacier face, and hence melting of ice by the ocean, is significantly increased via entrainment with rising turbulent plumes of buoyant subglacial water (SGW), which is ice sheet runoff emerging from cavities at the grounding line [*Holland et al.*, 2008; *Rignot et al.*, 2010; *Straneo et al.*, 2013; *Christoffersen et al.*, 2011; *Xu et al.*, 2012; *Motyka et al.*, 2003; *Jenkins*, 2011]. Because much of the ice sheet loss in the last decades has been synchronous with temperature increases in the AW circulating in boundary currents around the island [*Holland et al.*, 2008; *Christoffersen et al.*, 2011; *Rignot et al.*, 2012], many posit that enhanced ice melt by a warmer ocean has been a primary driver of Greenland's accelerating ice loss [e.g., *Straneo et al.*, 2013]. Yet the details by which ice melting by the ocean affects glacier front stability and flow speed are poorly known in part because of a lack of observations of the fjord bathymetry, shape of the submerged ice faces, and spatial and temporal variations in ocean thermal forcing. Subsurface, near-vertical, frontal regions are difficult to observe from remote sensing platforms, and in situ measurements are challenging to obtain beneath hundreds of meters of seawater in poorly charted, ice infested fjords.

Here we present side-looking, MultiBeam Echo Sounding (MBES) observations of fjord bathymetry and submerged ice faces of three West Greenland glaciers collected in August 2012 and 2013. In many of these fjords, the data represent the first detailed description of the seafloor bathymetry in front of these glaciers and the first attempt at imaging the submerged calving faces. We compare our results with existing International Bathymetry Charts of the Arctic Ocean (IBCAO3.0) [*Jakobsson et al.*, 2012], calculations of the SGW channel pathways, and numerical simulations of ice-ocean interaction along ice margins. We conclude on the impact of ice-ocean interaction on glacier front position, stability, and mass balance.

2. Data and Methods

Swath bathymetry. We employ a Reson 8160 MBES system operating at 50 KHz, mounted at a 30° angle to provide a useable swath width of the submerged glacier faces extending from the seafloor to the sea surface. The tilting of the sonar sacrifices horizontal swath width to permit measurements from the sea surface to the seafloor. The Reson 8160 has a useful maximum depth of 3000 m in typical fjord conditions. The presence of

icebergs, bergy bits, and growlers negatively affects sonar retrievals. However, sonar retrieval errors are overcome by combining scans of the same location from different look angles—available from the winding ship tracks through debris-laden fjords. The MBES is operated with a NAVCOM 3050 differential GPS unit with submeter position accuracy and an Applanix POSMV inertial navigation system which provides real-time vessel attitude and position. The data are acquired using the Quality Integrated Navigation System software and processed using the CARIS HIPS software. Calibration of sound speed in water is performed using Conductivity Temperature Depth (CTD) data obtained at regular intervals during the cruise and by surveying a set of topographic features on the seafloor at different look angles. Seafloor bathymetry products are generated on a 20 m grid with a vertical precision varying from 1 m in the best condition to 3–5 m when the boat changes course rapidly to avoid collision with large pieces of floating ice. Fjord surveys are conducted at a vessel speed of 5 to 6 kt and a pulse repetition frequency of 1 Hz, while face mapping requires vessel speeds of 1 kt or less.

Study area. Three major glaciers investigated include, from south to north and low to high ice discharge: Kangilernata Sermia (69.9°N, 50.35°W), Store Gletscher (70.38°N, 50.59°W), and Rink Isbræ(71.74°N, 51.65°W) (Figure 1). Bathymetry and face mapping were also conducted on Eqip Sermia (69.78°N, 50.25°W), Sermilik (70.62°N, 50.63°W), and Perdlerfiup Sermia (70.99°N, 50.9°W) but the data reveal that these glaciers are grounded at the end of deep fjords (400–900 m) on shallow plateaus (30–180 m). Consequently, they are not sufficiently deep to penetrate through the cold, fresh PW layer into the layer of warm, salty AW layer (Figure S1 in the supporting information). Our discussion focuses on the first three glaciers.

Hydrological modeling. We calculate the pathways of SGW using an hydrological model constrained by a 90 m Greenland Mapping Project (GIMP) digital elevation model [*Howat et al.*, 2014] and a 90 m bed topography reconstructed combining ice sounding radar and ice motion vectors [*Morlighem et al.*, 2014]. The hydrological model calculates the flow direction at each grid cell assuming that water is at the ice overburden pressure and that water flows downslope to an adjacent grid cell. SGW production is from ice sheet runoff reconstructed by RACMO [*Ettema et al.*, 2009]. Assuming that runoff immediately penetrates the ice through cracks and moulins to reach the bed, the SGW flow rate at each grid cell is the integrated upstream SGW flow [*Schwanghart and Scherler*, 2014]. The algorithm calculates the location and flux of SGW channels at the ice front. In the terminal valleys, we downscale the 11 km RACMO results to 90 m using the GIMP digital elevation model by forming a regional regression between runoff and surface elevation. Downscaling increases runoff production by 18 % on Store and Kangilernata and 0% on Rink and yields secondary SGW channels at the ice front, but most (> 90%) SGW flow remains confined in one or two channels.

Simulations of ice melt. We employ the Massachusetts Institute of Technology general circulation model (MITgcm) to simulate ice melt along a 150 m wide vertical ice face with a depth of 800 m below sea level (corresponding to the geometry of Rink), at 1 m horizontal and vertical resolution and a single SGW cavity [*Xu et al.*, 2013]. The results obtained for a 150 m wide section are then scaled to the entire glacier width. The open ocean boundary is constrained by a CTD profile acquired in August 2013 (Figure S2). Prior simulations indicate that changing the shape or number of SGW cavities for a constant SGW flux, Q_{sg}, changes the area-average melt rate of the ice face, Q_m, by less than 15%. In the case of Store, the model simulations have been successfully compared with melt rates calculated from an hydrographic survey [*Xu et al.*, 2013]. The SGW channel is 1 m in height, with a water flow speed of 0.5 m/s, and a width varying from 1 m to 60 m to simulate variations in Q_{sg} ranging from 0.5 m^3/s, typical of winter, to 30 m^3/s, typical of maximum summer rate. Thermal forcing, T_f, is 4°C. T_f is the depth-averaged difference between sea water temperature and its in situ freezing point. Prior simulations indicate a linear dependence of the melt rate, Q_m, with T_f and a sublinear dependence with Q_{sg}, i.e., $Q_m \propto T_f\, Q_{sg}^{\beta}$, where $\beta < 1$. We calculated Q_m averaged over the portion of the ice above the SGW channel (maximum melt) and the horizontally averaged Q_m over the entire 150 m wide face (average melt). Each sensitivity experiment is run for 6 h to ensure that the turbulent plume and ice melt rates achieve statistical equilibrium.

3. Results

Kangilernata Sermia flows into Atasund fjord which is connected to Disko Bay to the south via a 250 m deep sill (Figure 1a). The glacier drains a sector 7940 km^2 in size with a total mass accumulation of 1.35 Gt/yr. The ice front discharge increased from 0.9 Gt/yr in 1992 to 2.4 Gt/yr in 2011 or 80% above that required to maintain the glacier in a state of mass balance. Landsat time series imagery indicate that the ice front was stable in

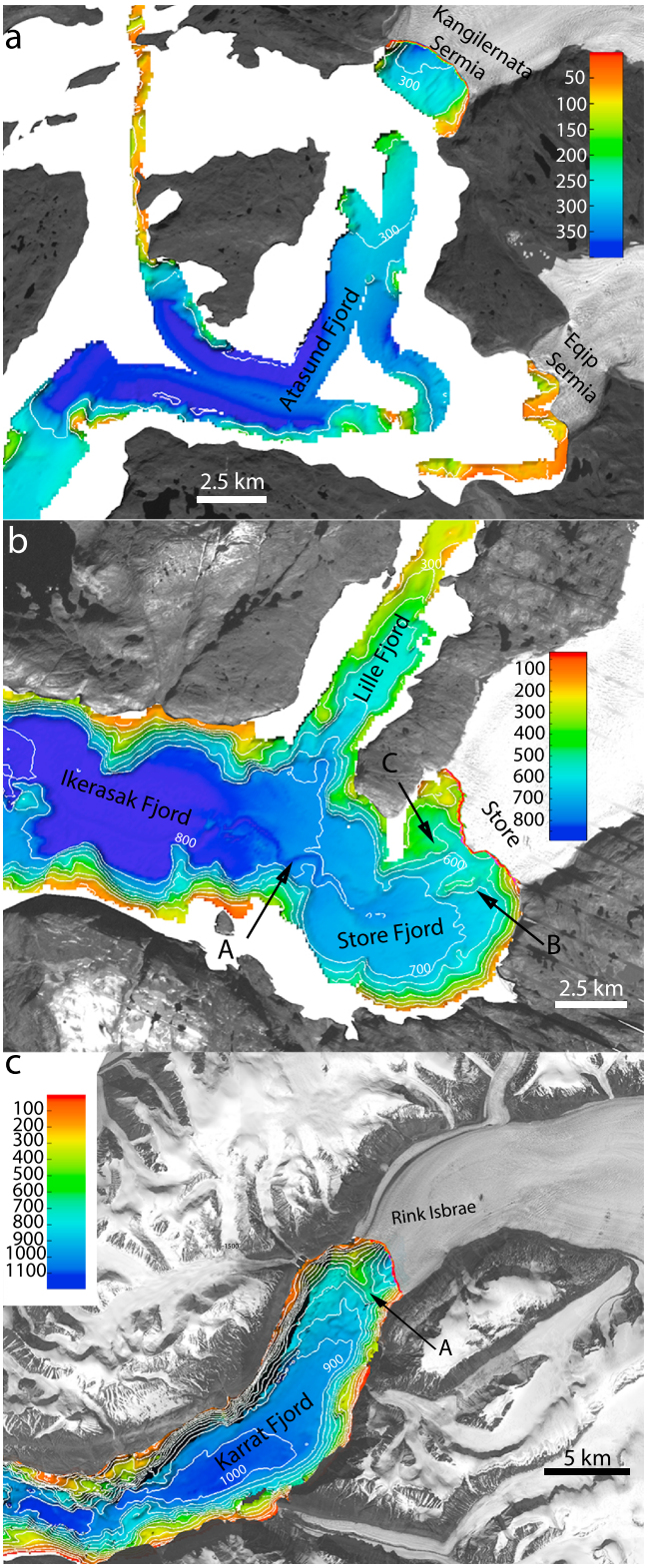

Figure 1. Seafloor bathymetry at (a) Kangilernata Sermia, (b) Store Gletscher, and (c) Rink Isbræ, West Greenland from MultiBeam Echo Sounding (MBES) in August 2012 and 2013, with Landsat 8 images for background. White areas have no MBES data. Bathymetric contours are 100 m. Locations A-C are discussed in the text. Projection is UTM zone 22, with north up.

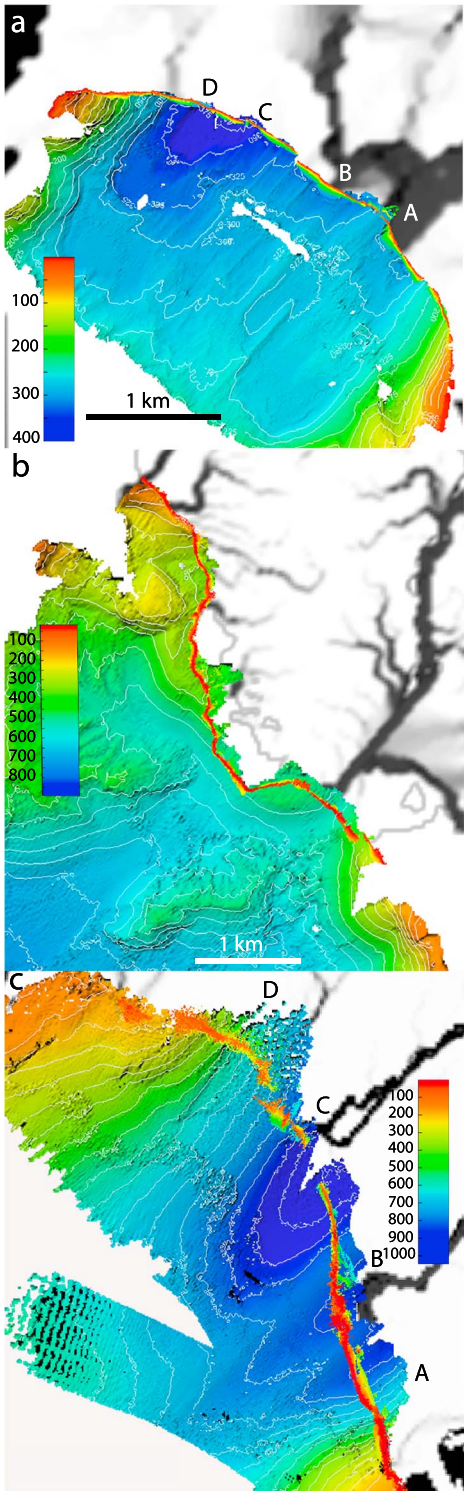

Figure 2. Vertical view of the seafloor bathymetry in front of (a) Kangilernata Sermia, (b) Store Gletscher, and (c) Rink Isbræ, West Greenland from MBES data with subglacial water (SGW) channels predicted by the hydrological model in black. Ice front elevations draped on the seafloor mark the ice front position at the sea surface for comparison with the extent of seafloor mapping by MBES data. Bathymetric contours are 50 m. White areas have no MBES data or SGW flow.

1964–1999 and retreated by 3 km in 1999–2014 (Figure S1). The annual frontal speed across the calving face averaged 2.2 m/d in 2008–2010 or 800 m/yr.

The MBES data reveal that the seafloor in front of Kangilernata is a classic U-shaped fjord with an average depth of 300 m and a maximum depth of 380 m on the northern flank (Figure 2a). The calving cliff is 50 m in height above sea level and no part of the glacier is afloat. Drumlins and glacial lineations 15 m in height and 200 m in width are found on the seafloor in front of the glacier in a zone that was covered by ice in 2005. Along the ice face, we detect a 250 m high, 500 m wide, and 150 m deep cavity at location A (Figure 3a). This cavity corresponds to the main SGW outflow manifest at the sea surface as a turbulent plume of sediment-laden water. Its position coincides with that predicted by the hydrostatic model. Near channel A and subchannels C and D, the seafloor mapping extends inland of the ice front position at the sea surface, i.e., the glacier face is undercut. The upper 100–200 m of the ice face are near vertical, and the lower part is undercut. Undercutting affects 76% of the glacier face, with an average cut of 30 m, or 11% of the glacier depth, and a maximum of 150 m at A (Figure 3a). Conversely, at locations such as B, the submerged calving cliff projects seaward of the subaerial ice front position by about 30 m (Figure S4).

Store Gletscher flows into Ikerasak fjord (Figure 1b), a 6 km wide, steep-walled fjord. The glacier annual frontal speed across its calving front is 9 m/d, which is the fifth fastest speed in Greenland [*Rignot and Mouginot*, 2012]. The glacier drains an area of 30,466 km^2 with a balance discharge of 8.7 Gt/yr. Its ice discharge of 11.0 Gt/yr in 2008–2011 was 10% larger than in 1992. The ice front position has not changed since 1948 (Figure S1).

Ikerasak fjord is 850 m deep on average and relatively flat which is indicative of extensive sediment deposits. To the west, the fjord overdeepens to 1400 m toward Uummannaq Island. To the east, rocky mounds 100–200 m in height and a few kilometers in diameter emerge from the sediment deposits. At the fjord center near location A, the data reveal a submarine channel, 50 m in height by 300 m in width, that extends more than 30 km from the glacier face into the fjord. We attribute its formation to turbidity current associated with downslope flow of dense, sediment-rich water [*Dowdeswell et al.*, 2014]. The fjord depth increases to 280 m to the north toward Lille Glacier and remains 500 m deep to the east toward Store Gletscher.At location B, we detect a sedimentary wedge, 150 m in height

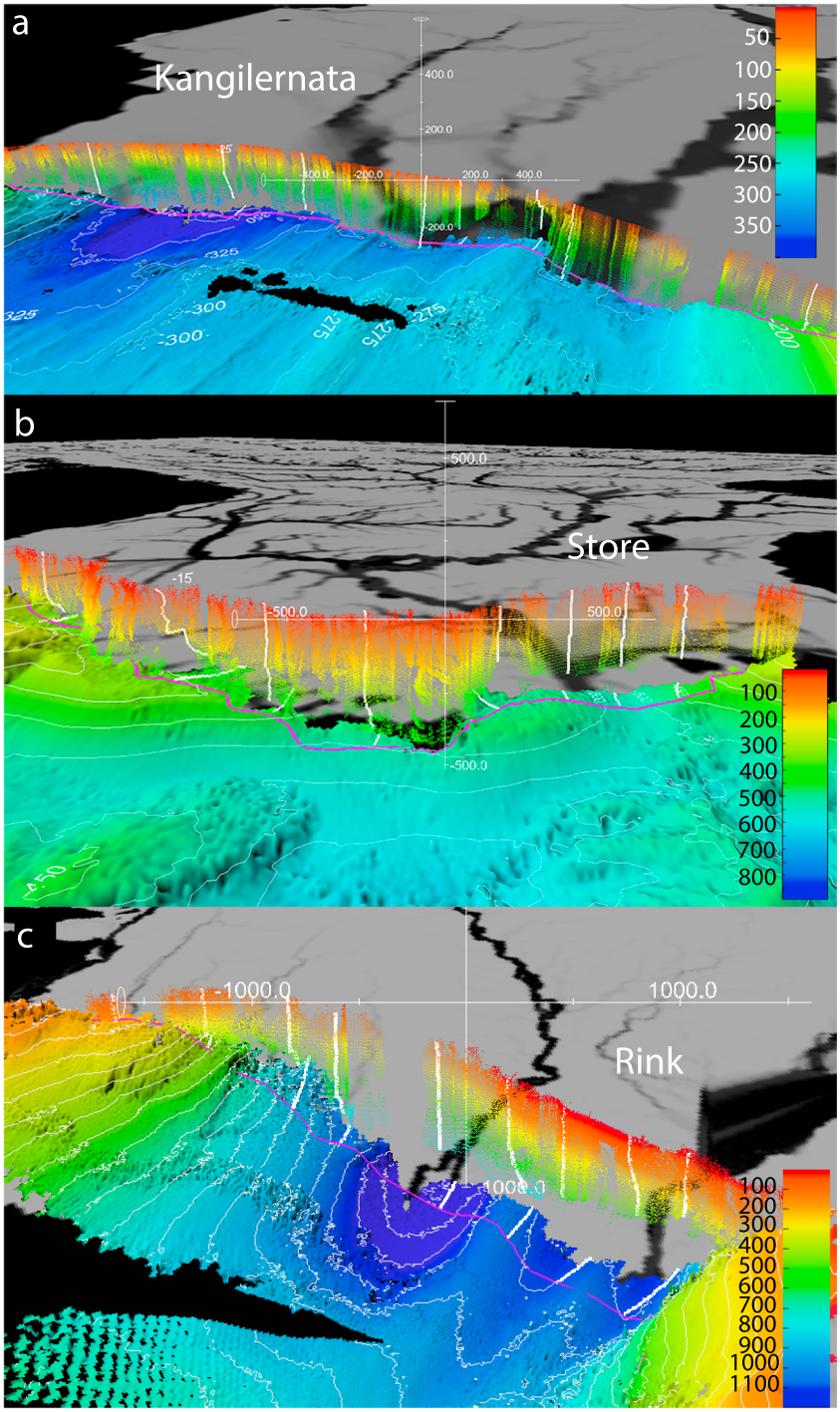

Figure 3. Point cloud representation of the calving faces of (a) Kangilernata Sermia, (b) Store Gletscher, and (c) Rink Isbræ, West Greenland, with MBES seafloor bathymetry and SGW outflow channels as in Figure 2. Posting is 20 m. Vertical exaggeration is 1.0. The purple line on the seafloor marks the position of the ice front at the sea surface. Seafloor mapping extends inland of that line due to glacier undercutting. Semi-regularly spaced vertical lines mark vertical profiles extending from the sea surface to the seafloor to facilitate visualization of the 3-D ice faces (see Figure S4).

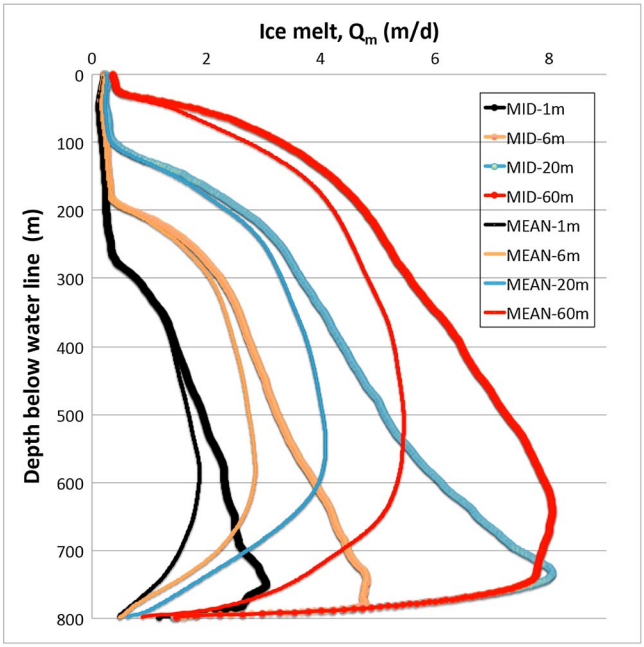

Figure 4. MITgcm simulations of ice melt rate, Q_m, in meter per day (m/d), for a 150 m wide × 800 m high vertical face versus depth below the sea surface for thermal forcing of $T_f = 4°C$, and one subglacial water (SGW) channel 1 m in height with a flow speed of 0.5 m/s. By varying the channel width from 1 m, 6 m, 20 m, and 60 m, we vary the SGW flux, Q_{sg} = 0.5, 3, 10, and 30 m^3/s. Q_{sg} = 0.5 m^3/s for winter and 60 m^3/s at maximum summer melt. Thin line is Q_m averaged over the entire face versus depth (mean). Thick line is Q_m averaged only above the SGW channel or maximum melt rate (mid).

by 200 m in width, up fjord of the main SGW channel at location C (Figure 2b). The location of the main SGW channel at C is consistent with surface observations and with the hydrological model. The seafloor is 560 m deep at the glacier center. The bed drops by several hundred meters both seaward and landward of the ice front, i.e., the glacier front is grounded on a sill plateau 560 m deep, 2 km long, that spans the entire glacier width. In 2013, we found that the central part of the ice front extended 420 m seaward of the 2012 position, with an ice draft 25–30 m above the seafloor (i.e., floating) versus a grounded ice front in 2012. This suggests that a small floating section periodically forms at the glacier center at the edge of the sill plateau. We posit that this configuration may help stabilize the glacier front because floating sections forming as the glacier advances are unsupported by glacier sides or small islands and therefore break up rapidly from buoyancy forces [e.g., *James et al.*, 2014].

A vertical view of the ice front reveals that the seafloor is imaged inland of the ice front position at the sea surface (purple line in Figure 3b), i.e., the ice face is undercut. The deepest zones of undercutting are found along the SGW channels (Figure 2b). About 27% of the ice face is projecting seaward of the subaerial ice front position, with an ice foot projecting by 26 m on average. The remaining 73% of the ice front is undercut on average by 100 m, with a maximum of 350 m at location D. Undercutting averages 30% of the glacier depth and is 3 times larger than on Kangilernata (Figure S4).

Rink Isbræ flows into Karrat fjord, at the northern end of Uummannaq fjord, with an annual frontal speed across the glacier width of 8 m/d, or the sixth fastest speed in Greenland (Figure 1c). Its drainage area of 33,171 km^2 (or 2% of Greenland) has a balance discharge of 11.7 Gt/yr. The ice front discharge increased from 11.7 Gt/yr in 1996 to 15.0 Gt/yr in 2011, hence 30% out of balance in 2011. The glacier front location has been stable over the past 40 years.

The seafloor in front of Rink exceeds 980 m depth at the center over a zone more than 2 km wide. The bed slowly rises to 200 m depth along the sides of the 5 km wide front (Figure 1c). A sill is present 10 km downstream of the 2013 ice front, with a depth varying from 350 to 650 m going from north to south [*Dowdeswell et al.*, 2014]. At locations A–D, where the hydrological model predicts SGW outflow, we observe deep glacier undercutting. In contrast with the other glaciers, undercutting affects almost the entire glacier face (Figure 3c).

The upper 300–400 m of the ice cliff are near vertical; the lower part is eroded by several hundred meters. Between A and C, the ice draft is 400 m deep, the glacier surface is near hydrostatic equilibrium and remains so for more than 1 km inland, i.e., the glacier forms a small floating section. Beyond C, the ice is depressed by a few tens of meters below hydrostatic equilibrium, the ice draft dips toward the seafloor, and the ice cavity is narrow (Figure S4). In total, undercutting averages 200 m, twice more than for Store, 30% of the glacier depth, with a maximum of 550 m at location D.

The MITgcm simulations reveal that maximum melt occurs in the lower part of the ice face, in the region directly above the SGW cavity (Figure 4). Ice melt decreases rapidly away from the cavity. The horizontally averaged melt rates are half as much than the maximum melt rates calculated in the region above the cavity. Almost no melt occurs near the surface. Melt rates reach several meters per day on the submerged ice faces. Ice melt rates increase sublinearly with Q_{sg}. Melt rates are largest when Q_{sg} is high, i.e., in the summer. Winter melt rates, which correspond to low Q_{sg} values, are 1 order of magnitude lower. Simulations conducted for shallower ice faces (300 m, 500 m) by *Xu et al.* [2013] yield similar sensitivity curves, which suggest that the results are not strongly dependent on the depth of the glacier.

4. Discussion

Swath bathymetry. The MBES data indicate that the surveyed fjords are significantly deeper than represented in the IBCAO [*Jakobsson et al.*, 2012]. IBCAO reports a maximum fjord depth of 150 m for Kangilnernata, 240 m for Rink, and 250 m for Store, with all three glaciers grounded at sea level (Figure S3). In contrast, the MBES data show that the fjords are hundreds of meters deeper and the glaciers are grounded 350 to 980 m below sea level. This discrepancy is explained by a lack of prior soundings in the fjords which results in sparse data being extrapolated to sea level along the fjord walls and along ice fronts in IBCAO. In IBCAO, the fjords would not be deep enough to host AW at these glacier termini. Yet CTD data collected in the fjords indicate the presence of AW (Figure S2).

Glacier undercutting. The MITgcm simulations explain the observed undercutting of ice faces at depth near the SGW channels and the presence of near-vertical ice faces away from the SGW channels and near the sea surface. Simulated vertically averaged melt rates are higher for Rink and Store than for Kangilernata because the latter is shallower (i.e., has a comparatively smaller proportion of its face in contact with AW) and has a much lower volume of SGW discharge. The results confirm the hypothesis that the cavities are generated by the efficient entrainment of ocean water in rising plumes, and consequent enhancement of melt rate.

An analysis of a forward ocean model along Greenland's coast at 4 km horizontal spacing, evaluated with in situ data, indicate that T_f may have increased by 1.0°C in Uummannaq Fjord since the 1990s [*Rignot et al.*, 2012]. During that time, ice sheet runoff doubled. When these numbers are used in our sensitivity analysis of ice melt derived from the MITgcm, we find that summer ice melt rates tripled for Kangilernata and increased by 50% for Store and Rink. For Kangilernata, this results in summer melt rates comparable in magnitude to the glacier frontal speed, hence capable of triggering a glacier front retreat, which is what happened in the 2000s. For Store and Rink, the enhanced melt rates remain one third to one fourth of the glacier frontal speed. We posit that this explains in part why Store and Rink have remained stable despite the calculated increase in ice melt by the ocean over the last two decades.

Subsurface undercutting reveals a fundamental process of ice-ocean interaction that has not been highlighted previously. It differs from ice melt at the water line for lake-terminating glaciers [*Benn et al.*, 2007], the buoyant flexure and fracture of semifloating sections at tide-water margins [*James et al.*, 2014], the viscous bending of ice shelf fronts caused by vertical differences between hydrostatic and seawater pressure [*Reeh*, 1968] or the fracturing of ice by tensile stresses and water propagating down cracks [*Benn et al.*, 2007]. Undercutting will alter the stress regime of the glacier front compared to that of a vertical face because it increases its bending moment. Bending and cracking are likely to operate on relatively short timescales, i.e., days to weeks because Q_m is measured in meters per day, whereas the viscous bending of ice operates on monthly time scales for a 400 m thick ice slab at −8°C [*Reeh*, 1968]. *O'Leary and Christoffersen* [2013] showed that undercutting causes calving to occur at significantly higher rates than for a vertical face, independent of the calving criterion used. The amplification of calving is most pronounced when undercutting takes place at depth, which is what we observe in our data. For calving events with a typical length of 0.3 to 1 times the ice thickness and wedge undercutting of the ice face, they report an amplification factor of 3 to 4. *Cook et al.* [2014] disputed *O'Leary and Christoffersen*'s [2013] results for not including viscous relaxation of the

bending moment but, as stated above, this relaxation probably operates on longer timescales. If *O'Leary and Christoffersen* [2013] are correct, the calving speed of undercut glaciers may approach and even exceed the ice frontal speeds, in which case the enhanced melting of the glaciers by the ocean will effectively result in a retreat of the ice front position. Further studies using the actual geometry of undercutting, precise ice surface elevation, ice temperature, and timescale of calving are needed to quantify the impact of undercutting on iceberg calving more completely.

Deep glacier undercutting may explain why most calving events take place above the sea surface rather than below in these fjords, because most submerged ice has already melted in the ocean. Undercutting may also explain the seasonal variability in calving speed noted elsewhere [e.g., *Sohn et al.*, 1998; *Luckman et al.*, 2006]. This seasonality has been attributed to the presence of a mechanically competent ice melange in winter which offers resistance to glacier flow even though the melange is often orders of magnitude thinner than the glacier front. We propose an alternative explanation. The MITgcm simulations indicate that in winter, when $Q_{sg} = 0$, the melt rates Q_m are 50 to 70% lower, hence calving should be less efficient and the ice front is more likely to advance. In that case, it may not be required to invoke a seasonal buttressing of the ice front by the ice melange, because ice-ocean interaction, undercutting, and therefore iceberg calving are significantly modulated by seasonal forcing in SGW outflow. We also note that as SGW outflow increases in a warmer climate, undercutting, calving and retreat rate will increase even if the temperature of the ocean remains the same.

5. Conclusions

Our MBES observations of three marine-terminating glaciers in West Greenland reveal fjords far deeper than reported in existing international digital charts, with rough and complex submerged ice faces that include wide cavities at the location of SGW outflow and associated large areas of glacier undercutting. Deep undercutting above the grounding line by warm AW entrained in rapidly ascending buoyant subglacial discharge-driven plumes is an important process of ice removal and destabilization of the glacier fronts that is not included in the current generation of numerical models of Greenland glacier dynamics [e.g., *Gillet-Chaulet et al.*, 2012] or weakly parameterized [*Nick et al.*, 2013]. These numerical models therefore neglect a major—perhaps even dominant—process of ablation controlled by ocean temperature and ice sheet surface runoff. Additional work is required to quantify the impact of glacier undercutting on glacier dynamics. Our results also illustrate the need to conduct widespread surveys of seafloor bathymetry and ocean temperature/salinity in the glacial fjords to better understand and study ice-ocean interaction. Such observations will help establish the pathways of AW toward the glaciers and their impact on ice calving and ice flow speed. As glaciers retreat, the SGW pathways, ice face melt rates, and calving rates will vary due to changes in ice thickness, cavity shape, and water temperature. Progress in numerical modeling of such a complex system therefore requires the development and usage of high-resolution, coupled, ice-ocean-atmosphere numerical models with adaptive geometries, and complete physics of ice-ocean interaction, including in turbulent plumes rising along a complex, undercut, rough ice-ocean interface. In the absence of such numerical models, we suggest that the sensitivity of Greenland glaciers to ocean warming and enhanced ice sheet runoff may have been underestimated and projections of sea level rise from the Greenland Ice Sheet will need to be revised upward.

Acknowledgments
This work was performed at the University of California Irvine under grant 3280 from the Gordon and Betty Moore Foundation, start up funds from UC Irvine, and grant NNX12AB86G from the National Aeronautics and Space Administration's Cryospheric Science Program and at the Jet Propulsion Laboratory, California Institute of Technology under a grant from NASA. IF's research was carried out in part by an appointment to the NASA Postdoctoral Program at the Jet Propulsion Laboratory, California Institute of Technology, administered by Oak Ridge Associate Universities through a contract with NASA and in part through NSFgrant ARC-1023499.

The Editor thanks Doug Benn for his assistance in evaluating this paper.

References

Benn, D. I., C. Warren, and R. H. H. Mottram (2007), Calving processes and the dynamics of calving glaciers, *Earth Sci. Rev.*, *82*, 143–179.
Christoffersen, P., et al. (2011), Warming of waters in an East Greenland fjord prior to glacier retreat: Mechanisms and connection to large-scale atmospheric conditions, *The Cryosphere*, 5(3), 701–714.
Cook, S., et al. (2014), Modelling environmental influences on calving at Helheim Glacier in eastern Greenland, *The Cryosphere*, *8*, 827–841.
Dowdeswell, J. A., K. A. Hogan, C. O. Cofaigh, E. M. G. Fugelli, and J. Evans (2014), Late quaternary ice flow in a West Greenland fjord and cross-shelf trough system: Submarine landforms from Rink Isbræto Uummannaq shelf and slope, *Quat. Sci. Rev.*, *92*, 292–309.
Ettema, J., M. R. van den Broeke, E. van Meijgaard, W. J. van de Berg, J. L. Bamber, J. E. Box, and R. C. Bales (2009), Higher surface mass balance of the Greenland ice sheet revealed by high-resolution climate modelling, *Geophys. Res. Lett.*, *36*, L12501, doi:10.1029/2009GL038110.
Gillet-Chaulet, F., O. Gagliardini, H. Seddik, M. Nodet, G. Durand, C. Ritz, T. Zwinger, R. Greve, and D. G. Vaughan (2012), Greenland ice sheet contribution to sea-level rise from a new-generation ice-sheet model, *The Cryosphere*, *6*, 1561–1576.
Holland, D. M., R. H. Thomas, B. de Young, M. H. Ribergaard, and B. Lyberth (2008), Acceleration of Jakobshavn Isbræ triggered by warm subsurface ocean waters, *Nat. Geosci.*, 1(10), 659–664.
Howat, I. M., A. Negrete, and B. E. Smith (2014), The Greenland Ice Mapping Project (GIMP) land classification and surface elevation datasets, *The Cryosphere*, *8*, 1509–1518.
Jakobsson, M., et al. (2012), The International Bathymetric Chart of the Arctic Ocean (IBCAO) version 3.0, *Geophys. Res. Lett.*, *39*, L12609, doi:10.1029/2012GL052219.

James, T. D., T. Murray, N. Selmes, K. Scharrer, and M. O'Leary (2014), Buoyant flexure and basal crevassing in dynamic mass loss at Helheim Glacier, *Nat. Geosci.*, *7*, 593–596.

Jenkins, A. (2011), Convection-driven melting near the grounding lines of ice shelves and tidewater glaciers, *J. Phys. Oceanogr.*, *41*(12), 2279–2294.

Luckman, A., T. Murray, R. de Lange, and E. Hanna (2006), Rapid and synchronous ice-dynamic changes in East Greenland, *Geophys. Res. Lett.*, *33*, L03503, doi:10.1029/2005GL025428.

Morlighem, M., E. Rignot, J. Mouginot, H. Seroussi, and E. Larour (2014), Deeply incised submarine glacial valleys beneath the Greenland Ice Sheet, *Nat. Geosci.*, *7*, 418–422.

Motyka, R. J., L. Hunter, K. A. Echelmeyer, and C. Connor (2003), Submarine melting at the terminus of a temperate tidewater glacier, LeConte Glacier, Alaska, U. S. A, *Ann. Glaciol.*, *36*, 57–65.

Nick, F. M., A. Vieli, M. L. Andersen, I. Joughin, A. Payne, T. L. Edwards, F. Pattyn, and R. S. W. van de Wal (2013), Future sea-level rise from Greenland's main outlet glaciers in a warming climate, *Nature*, *497*, 235–238.

O'Leary, M., and P. Christoffersen (2013), Calving on tidewater glaciers amplified by submarine frontal melting, *The Cryosphere*, *7*, 119–128.

Reeh, N. (1968), On the calving of ice from floating glaciers and ice shelves, *J. Glaciol.*, *7*(50), 215–32.

Rignot, E., M. Koppes, and I. Velicogna (2010), Rapid submarine melting of the calving faces of west Greenland tidewater glaciers, *Nat. Geosci.*, 3(3), 187–191.

Rignot, E., I. Velicogna, M. van den Broeke, and A. Monaghan (2011), Acceleration of the contribution of the Greenland and Antarctic ice sheets to sea level rise, *Geophys. Res. Lett.*, *38*, L05503 doi:10.1029/2011GL046583.

Rignot, E., and J. Mouginot (2012), Ice flow in Greenland for the International Polar Year 2008–2009, *Geophys. Res. Lett.*, *39*, L11501, doi:10.1029/2012GL051634.

Rignot, E., I. Fenty, D. Menemenlis, and Y. Xu (2012), Spreading of warm ocean waters around Greenland as a possible cause for glacier acceleration, *Ann. Glaciol.*, 53(60), 257–266.

Schwanghart, W., and D. Scherler (2014), TopoToolbox 2 MATLAB-based software for topographic analysis and modeling in Earth surface sciences, *Earth Surf. Dyn.*, *2*, 1–7.

Sohn, H. G., K. C. Jezek, and C. J. van der Even (1998), Jakobshavn Glacier, West Greenland: 30 years of spaceborne observations, *Geophys. Res. Lett.*, 25(14), 2699–2702.

Straneo, F., et al. (2013), Challenges to understand the dynamic response of Greenland's marine terminating glaciers to oceanic and atmospheric forcing, *Bull. Am. Meteorol. Soc.*, 94(8), 1131–1144.

Xu, Y., E. Rignot, D. Menemenlis, and M. Koppes (2012), Numerical experiments on subaqueous melting of Greenland tidewater glaciers in response to ocean warming and enhanced subglacial runoff, *Ann. Glaciol.*, 53(60), 229–234.

Xu, Y., E. Rignot, I. Fenty, D. Menemenlis, and M. Mar Flexas (2013), Subaqueous melting of Store Glacier, West Greenland from three-dimensional, high-resolution numerical modeling and ocean observations, *Geophys. Res. Lett.*, *40*, 4648–4653, doi:10.1002/grl.50825.